International Journal of Thermophysics, Vol. 22, No. 3, 2001

A Study of Lennard–Jones Equivalent Analytical Relationships for Modeling Viscosities

M. S. Zabaloy,[1,2] J. M. V. Machado,[1] and E. A. Macedo[1,3]

Received July 21, 2000

An analytical representation of the viscosity–density–temperature relationship of the Lennard–Jones (LJ) fluid, over wide ranges of temperature and density, is critically assessed and combined with an LJ pressure–density–temperature equation of state to allow LJ viscosity calculations at a given temperature and pressure. Both LJ equivalent analytical relationships (EARs) are accurate. The potential of using an LJ-based model to represent the viscosities of real fluids is evaluated in two steps. First, the qualitative trends generated by the two combined LJ EARs are studied. Second, viscosity predictions for real, relatively simple, fluids are performed. For these, it is assumed that a real fluid behaves as an LJ fluid having a critical temperature T_c and a critical pressure P_c exactly matching the real-fluid experimental values of T_c and P_c. Such an assumption is equivalent to supposing that real fluids behave as LJ fluids with effective intermolecular potential parameters consistent with the experimental critical coordinates. The viscosity predictions are based only on molecular weight, T_c, and P_c. The quantitative evaluation is relative to a database of 30 relatively simple compounds including 4 noble gases and the olefinic and aliphatic straight-chain hydrocarbons through 8 carbon atoms. Conditions for the evaluation ranged from 0.6 to 3 for reduced temperatures and from 0 to 3 for LJ reduced densities. The average error is usually less than 10% for vapor and supercritical viscosity and usually less than 25% for liquid viscosity. In its present form, the methodology is actually a corresponding-states model where the reference fluid is an LJ fluid.

KEY WORDS: dense fluids; gases; Lennard–Jones; modeling; molecular theory; viscosity.

[1] LSRE—Laboratory of Separation and Reaction Engineering, Departamento de Engenharia Química, Faculdade de Engenharia, Universidade do Porto, Edifício E, Rua Dr. Roberto Frias s/n, 4200-465 Porto, Portugal.

[2] To whom correspondence should be addressed. E-mail: eamacedo@fe.up.pt

[3] Permanent address: Planta Piloto de Ingenieria Química—PLAPIQUI (UNS-CONICET), Camino La Carrindanga Km 7, 8000 Bahia Blanca, Argentina.

0195-928X/01/0500-0829$19.50/0

1. INTRODUCTION

Model fluids are imaginary substances that have a well-defined expression for the intermolecular potential. The values of the properties of model fluids, under given input conditions, are obtained through computer experiments using methods such as molecular dynamics (MD) [1]. Once good-quality computer simulation data are available for a chosen model fluid, over a wide enough range of conditions, they can be summarized in the form of equivalent analytical relationships (EARs). EARs are analytical functions that, from the same input information used to run a computer experiment, provide values for the model fluid properties which agree well with those of the actual computer experiment.

Simulated data correspond to substances which obey strictly a prescribed intermolecular potential model. Therefore, simulated data on a chosen model fluid are conventionally used for studying fundamental issues such as the extension of measurements to regions not accessible to experiments or the correct form for mixing rules (e.g., Ref. 2). Real fluids behave according to the complex intermolecular interactions of real molecules, whatever their mathematical form may be, rather than according to the relatively crude intermolecular potential forms of well-known model fluids. In spite of this, simulated data or their corresponding EARs have also been used as the basis for engineering models applicable to real fluids. For instance, Sun and Teja [3] have modeled the vapor–liquid equilibria of systems containing polar or elongated molecules using a Lennard–Jones (LJ) equation of state (EOS) with temperature-dependent effective LJ parameters. In this case, all the complex interactions taking place between real nonspherical molecules, often with the presence of polar or specific intermolecular forces, are lumped into a single pseudo-LJ intermolecular potential. This approach is acceptable for engineering calculations, and we adopt it in the present work. Sun and Teja [3] applied their LJ EOS for mixtures using the van der Waals (VW) one-fluid mixing rules. These researchers [3] found that their LJ + VW EOS could be used to correlate as well as to extrapolate mixture data over considerable ranges of temperature and pressure and also found, on the other hand, that commonly used purely empirical EOS models were inadequate when extrapolated. The systems studied [3] contained molecules of considerable complexity (e.g., water, ethanol, methane, *n*-decane), and the pure-compound LJ parameters were made temperature dependent. Despite the non-LJ nature of the studied complex molecules, Sun and Teja [3] concluded that the predictive power is higher for LJ-based EOSs than for cubic EOSs. The most probable explanation for these conclusions is that LJ EOSs acknowledge the existence of discrete

molecules through forced agreement with results from molecular-level computer experiments, rather than assuming that fluids have a continuous nature. Results such as those of Sun and Teja [3] indicate that engineering models based on computer experiments have a greater potential than purely empirical correlations to represent accurately the properties of real fluids, as long as the chosen model fluid is realistic. A purely empirical correlation is, on the other hand, a model that does not specify an intermolecular potential function (macroscopic approach) [4]. The techniques of Ref. 3 show how the LJ fluid can encapsulate not only the behavior of simple substances but also the behavior of complex real fluids, if proper corrections are introduced.

To generate a model applicable to engineering calculations, the choice of a suitable model fluid should be guided by the following requirements: (a) ability to represent well the essential behavior of real fluids, (b) availability of computer simulation data over wide ranges of pressure and temperature to build proper EARs, and (c) relative simplicity of the intermolecular potential function. With respect to the first requirement, the intermolecular potential function u and its derivatives with respect to the intermolecular distance r should preferably be continuous functions of r. The well-known LJ model fluid fulfills, in principle, all these prerequisites.

The physical property of focus in the present work is the Newtonian shear viscosity. Our long-term goal is to develop a model applicable over wide ranges of temperature and pressure, with special emphasis on the dense region. However, the model should also provide reasonable viscosity values for low-density fluids. Hence, a unified treatment of all possible fluid phase states, such as liquid, vapor, and supercritical fluid, is required. This is also a precondition for the description of asymmetric mixtures. The model has to be based on molecular theory and should take advantage of recent EARs and/or computer simulation data. Besides, the computation time should be compatible with engineering needs. Hence, a good balance between accuracy and simplicity should be reached. Additionally, the required experimental input information should be kept to a minimum.

Toward these goals, the purpose of the present work is to evaluate the potential of combining existing LJ EARs for representing the viscosities of real fluids. We review the relevant literature and test the consistency among previous works by different authors. In view of our objectives, some simplifications are proposed. Afterward, the potential of the new modeling approach is assessed by looking at the qualitative trends for viscosity over wide ranges of temperature and pressure and by the quantitative comparison of predicted and experimental viscosities.

2. THE LENNARD–JONES (LJ) FLUID

The expression for the LJ intermolecular potential is the following:

$$u(r) = 4\varepsilon \left[\left(\frac{\sigma}{r} \right)^{12} - \left(\frac{\sigma}{r} \right)^{6} \right] \tag{1}$$

where r is the intermolecular distance, u is the potential energy, ε is the depth of the LJ potential well, and σ is the LJ separation distance at zero energy.

The LJ reduced temperature T^+, reduced pressure P^+, reduced density ρ^+, and reduced viscosity η^+ are conventionally defined as follows:

$$T^+ = \frac{kT}{\varepsilon} \tag{2}$$

$$P^+ = \frac{P\sigma^3}{\varepsilon} \tag{3}$$

$$\rho^+ = \frac{N}{V}\sigma^3 = N_{\mathrm{A}}\rho\sigma^3 \tag{4}$$

$$\eta^+ = \eta \frac{\sigma^2}{\sqrt{m\varepsilon}} \tag{5}$$

where k is the Boltzmann constant, T is the absolute temperature, P is the absolute pressure, N is the number of molecules, V is the system volume, N_{A} is Avogadro's number, ρ is the amount-of-substance density, η is the Newtonian shear viscosity, and m is the mass of one molecule. The variable ρ^+ is not necessarily limited to values less than unity.

Rowley and Painter (RP) [5] computed LJ shear viscosities under 171 conditions covering a wide range of density and temperature, using the method of molecular dynamics. They fitted the following equivalent analytical relationship (EAR) to the simulation data, which makes it possible to calculate viscosities analytically from the values of T^+ and ρ^+:

$$\eta^+ = \eta_0^+ \exp\left[\sum_{i=1}^{4} \sum_{j=1}^{6} b_{ji} \frac{(\rho^+)^i}{(T^+)^{(j-1)}} \right] \tag{6}$$

with

$$\eta_0^+ = \frac{5}{16}\sqrt{\frac{T^+}{\pi}} \left(\sum_{j=1}^{5} \omega_j (T^+)^{(j-1)} \right)^{-1} \tag{7}$$

where η_0^+ is the LJ reduced viscosity limit at zero density. The values of the coefficients b_{ji} and ω_i were provided in Ref. 5 except for two errors on parameters b_{32} and ω_2. Their proper values are $b_{32} = 1067.97$ and $\omega_2 = -2.0265$ [16]. We identify this set of parameter values as the original RP set of parameters b_{ji} and ω_i.

The RP viscosity equation of state, i.e., Eq. (6), has the temperature range of application $0.8 \leqslant T^+ \leqslant 4$. The range for ρ^+ is from 0 to the minimum between 1 and the density of the dense LJ fluid in equilibrium with the LJ solid ($\rho^+_{\text{fluid, SFE}}$). Throughout the present article any reference to solid–fluid equilibrium (SFE) excludes the equilibrium between the solid and a low-density vapor (i.e., the sublimation equilibrium is excluded).

Viscosity diverges at the critical point [6]. Equation (6) does not account for the critical enhancement for viscosity that takes place in the neighborhood of the critical point. In contrast with the case of thermal conductivity, the critical enhancement in viscosity is small and becomes important only within a narrow region around the critical point [6]. Watson et al. [7] presented a clear illustration of the critical enhancement effect. They also argued in favor of the viscosity factorization of Eq. (6), as opposed to an additive representation expressing the dense fluid viscosity as the summation of the zero-density viscosity plus a residual term.

The usual engineering need is to calculate viscosities at a given temperature and pressure. Hence, we need an LJ EAR, connecting the temperature, the pressure, and the density, which could be combined with Eq. (6). Kolafa and Nezbeda (KN) [8] proposed one such analytical EOS for the LJ fluid: the PVE/hBH LJ EOS. This EOS is based on a perturbed virial expansion with a theoretically defined temperature-dependent reference hard-sphere term. The PVE/hBH LJ EOS is based on critically assessed computer simulation data from several sources. The good quality of this LJ EOS was confirmed by Mecke et al. [9].

The PVE/hBH LJ EOS is

$$z = \frac{P^+}{\rho^+ T^+} = f_{\text{KN}}(\rho^+, T^+) \tag{8}$$

where z is the compressibility factor and f_{KN} is a function of ρ^+ and T^+ defined in Appendix A. The temperature range of application of Eq. (8) is $0.68 \leqslant T^+ \leqslant 10$. The range for ρ^+ is from 0 to the density of a dense LJ fluid in equilibrium with an LJ solid ($\rho^+_{\text{fluid, SFE}}$).

Kolafa and Nezbeda [8] built Eq. (8) without imposing constraints related to the location of the critical point. Hence, the PVE/hBH EOS is a classical LJ EOS. The critical coordinates corresponding to Eq. (8) are the following [8]:

$$T_c^+ = 1.3396 \tag{9}$$

$$P_c^+ = 0.1405 \tag{10}$$

$$\rho_c^+ = 0.3108 \tag{11}$$

$$z_c = 0.3375 \tag{12}$$

It can be shown that, in spite of the noncubic nature of the PVE/hBH LJ EOS, Eq. (8), the number of ρ^+ values compatible with given physically meaningful values of T^+ and P^+ never exceeds three, as in the case of semiempirical cubic EOSs (e.g., Ref. 10), as long as Eq. (8) is used within its range of applicability. At subcritical temperatures, the number of ρ^+ values compatible with a given P^+ value can be quickly established using the techniques of Ref. 11.

The availability of a procedure to compute $\rho^+_{\text{fluid, SFE}}$ is required to use Eqs. (6) and (8) properly. Agrawal and Kofke [12] reported properties of the LJ fluid at solid–fluid coexistence from the LJ triple-point temperature up to temperatures much higher than the vapor–liquid LJ critical temperature. Agrawal and Kofke [12] provided the following semiempirical fit of the melting line:

$$P^+_{\text{SFE}} = \beta^{-5/4}(A + B\beta + C\beta^2)\exp(-D\beta^{1/2}) \tag{13}$$

where P^+_{SFE} is the melting pressure P^+ and

$$\beta = \frac{1}{T^+} \tag{14}$$

The parameters of Eq. (13) are given in Table I [12].

Equation (13) is an EAR that corresponds both to the solid–liquid equilibrium and to the solid–supercritical fluid equilibrium. Equation (13) is not valid for the LJ solid–vapor equilibrium that takes place at temperatures lower than the LJ triple-point temperature. The range of Eq. (13) is $0.00365 \leqslant \beta \leqslant 1.456$, which corresponds to the (wide) T^+ range $0.686813 \leqslant T^+ \leqslant 273.973$. At a given value of T^+, the pressure of LJ solid/dense-fluid equilibrium can be computed using Eq. (13). The resulting value of

Table I. Parameters in Eq. (13)

A	16.89
B	−7.19
C	−3.028
D	0.4759

P^+ can then be introduced into Eq. (8) to calculate the dense fluid ρ^+ value. The ρ^+ values obtained in this way, for a range of values of T^+, should be equal to the values of $\rho^+_{\text{fluid, SFE}}$ reported by Agrawal and Kofke [12]. Figure 1 shows such a comparison. The solid line corresponds to calculated values of $\rho^+_{\text{fluid, SFE}}$, while the squares correspond to the LJ fluid density data of Agrawal and Kofke [12]. From this figure it is clear that there is a very good agreement between Ref. 8 and Ref. 12. Figure 1 also shows the LJ data for the saturated solid and for the LJ fluid under conditions of vapor–liquid equilibrium. The horizontal and vertical simple dashed lines and the solid line define the limits of applicability of Eq. (6). The two horizontal compound-dashed lines and the solid line define the

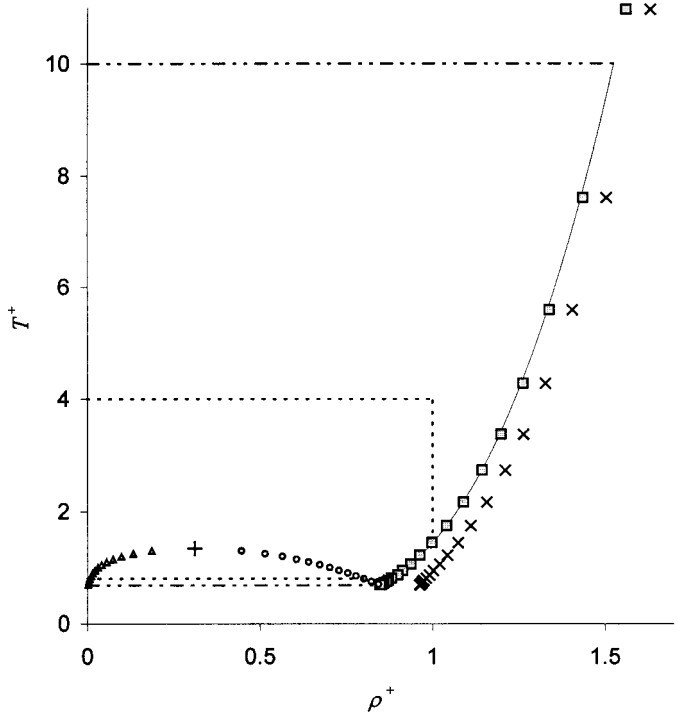

Fig. 1. Temperature–density phase diagram for the Lennard–Jones (LJ) fluid. Solid line: highest ρ^+ given by the PVE/hBH LJ equation of state, Eq. (8), at solid–fluid equilibrium P^+ [Eq. (13)]. (×) LJ solid density data at solid–fluid equilibrium [12]; (□) LJ fluid density data at solid–fluid equilibrium [12]; (○) PVE/hBH LJ EOS VLE liquid density calculated by Mecke et al. [9]; (△) PVE/hBH LJ EOS VLE vapor density calculated by Mecke et al. [9]; (+) LJ critical point according to Eqs. (9) and (11).

limits of applicability of Eq (8). The range of the PVE/hBH LJ EOS completely contains the range of the RP viscosity EAR.

In summary, the equations presented in this section make it possible to analytically calculate the LJ viscosity η^+ at a given temperature T^+ and pressure P^+, paying close attention to the ranges of applicability of the viscosity and pressure LJ-EARs.

3. THE MODIFIED LENNARD–JONES VISCOSITY EQUATION

The future development of the present work will require calculations of properties of real fluids based on LJ properties. Real-fluid conditions of temperature and pressure can make the required LJ computations fall outside the range of applicability of Eqs. (6) and (8). Hence, for such cases, proper extrapolation schemes will have to be set for computing LJ densities and viscosities. Equation (6), coupled with the original RP set of parameters b_{ji} and ω_i, gives a relatively complex viscous behavior at a low density and low temperature: a minimum appears for viscosity as a function of density. Such behavior complicates the setting of robust extrapolation schemes to be used at low temperatures. On the other hand, the effect is not quantitatively important. Hence, we modified slightly the model set by Eq. (6). The new form for the viscosity dependence on temperature and density is

$$\eta^+ = \eta_0^+ \exp\left[\sum_{i=2}^{4}\sum_{j=1}^{6} b_{ji}\frac{(\rho^+)^i}{(T^+)^{(j-1)}}\right] \tag{15}$$

where η_0^+ is given by Eq. (7), as in the original RP model. The difference between Eq. (6) and Eq. (15) is that in Eq. (15) all terms corresponding to $i=1$ have been removed; i.e., all terms linear in ρ^+ have been eliminated. This imposes the flatness of the η^+-vs-ρ^+ curve at $\rho^+=0$. The values of the b_{ji} parameters to be used in Eq. (15) are different from the original RP values. Table II presents the new set of b_{ji} parameters. We fitted the b_{ji}

Table II. Values for the Parameters of Eq. (15) Obtained in this Work

j	i	b_{ji}	j	i	b_{ji}	j	i	b_{ji}
1	2	0.7607120	1	3	0.4221662	1	4	−0.6411574
2	2	8.1770068	2	3	1.7296571	2	4	0.2811374
3	2	2.5445750	3	3	−14.372592	3	4	−5.1536547
4	2	−0.0532996	4	3	−9.3141867	4	4	26.873939
5	2	1.6436829	5	3	5.2107990	5	4	−15.182439
6	2	−1.2500496	6	3	0.9588608	6	4	1.7614285

parameters of Eq. (15) forcing the absence of minima for viscosity as a function of density and forcing the fulfillment of some suitable restrictions. This is acceptable for engineering purposes. We provide the details in Appendix B.

Now, our LJ viscosity EAR is defined by Eqs. (15) and (7), by the original RP ω_i parameters, and by the parameters reported in Table II. The temperature range of applicability is $0.8 \leqslant T^+ \leqslant 4$. The range for ρ^+ is from 0 to the minimum between 1 and the density of the dense LJ fluid in equilibrium with the LJ solid ($\rho^+_{\text{fluid, SFE}}$), computed as described in the previous section. The new set of equations and parameters will be our basic model for the results presented below and for the future continuation of the present work.

Appendix B provides information on the quantitative performance of Eq. (15), used with the parameters reported in Table II.

4. RESULTS: QUALITATIVE ASSESSMENT

Figure 2 shows, on the viscosity–pressure plane, the effect of combining the viscosity–temperature–density EAR, Eq. (15)/Table II, with the pressure–temperature–density EAR, Eq. (8), for the LJ fluid. For chosen

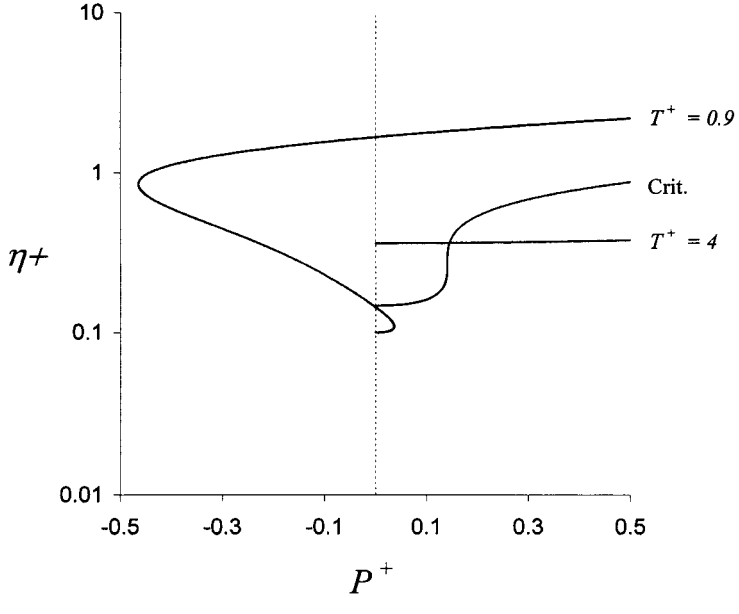

Fig. 2. Viscosity vs pressure for the Lennard–Jones fluid, as represented by Eqs. (15) and (7) coupled with Table II parameters and Eq. (8).

values of temperature T^+ and density ρ^+, the viscosity and the pressure are obtained from Eqs. (15) and (8), respectively, and plotted. For a given isotherm the computations are performed from zero density up to a high enough density (which is equal to, at most, the fluid density at SFE, $\rho^+_{\text{fluid, SFE}}$). The plot shows three isotherms. A region of negative pressure for the subcritical isotherm is the consequence of having used Eq. (8), which, in this respect, behaves as simpler analytical PVT EOSs. The critical isotherm shows a flat region where small changes in pressure produce important changes in viscosity. On the other hand, at very high temperatures, the LJ viscosity is much less sensitive to pressure. From Fig. 2 it is clear that the set of equations (15)–(8) can basically represent the viscosity of subcritical vapors and liquids, and of near-critical or supercritical fluids, over the whole pressure (density) range. The shape of the subcritical isotherm is a consequence in part of the restrictions described in Appendix B. If the viscosity had been allowed to have a minimum with respect to density in the low-density region, a more complicated shape for subcritical isotherms would have been obtained.

From Eq. (5) it can be shown that

$$\eta^+ = \eta_0^+ \frac{\eta}{\eta_0} \tag{16}$$

where η_0 is the value of η at zero density.

Also, from Eq. (3), we write

$$P^+ = P_r P_c^+ \tag{17}$$

where P_c^+ is a constant [Eq. (10)] and P_r is the practical reduced pressure, defined as

$$P_r = \frac{P}{P_c} \tag{18}$$

A chosen value of P_r sets a value for P^+ through Eq. (17). Using Eqs. (B1), (17), (7), and (15), with the parameters in Table II, and Eqs. (8) and (16), the plot in Fig. 3 can be generated. Figure 3 depicts the ratio of viscosity over zero-density viscosity (η/η_0) as a function of the reduced pressure P_r for the LJ fluid for different isotherms. Figure 3 agrees well with Fig. 1.3.2 in the classical book by Bird et al. [13].

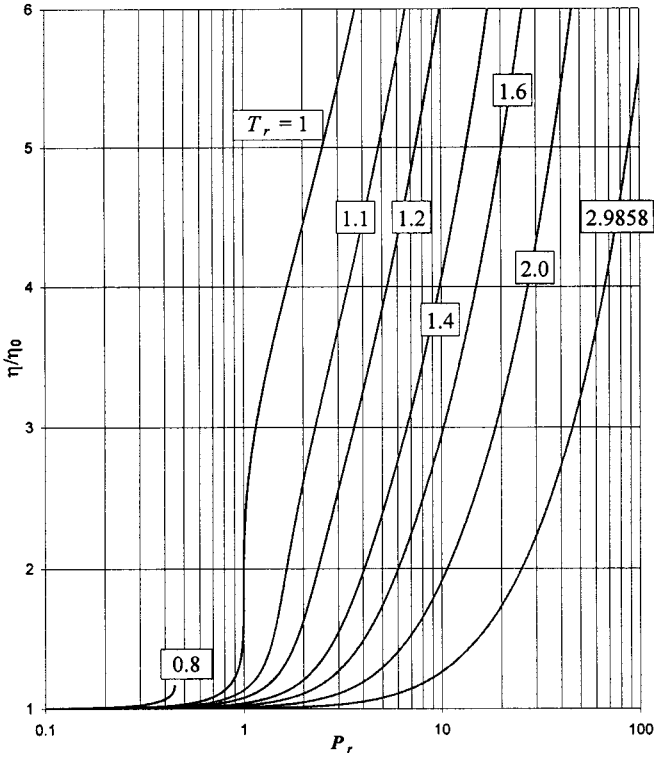

Fig. 3. Ratio of viscosity to zero-density viscosity (η/η_0) as a function of the reduced pressure P_r for the Lennard–Jones fluid.

From Eq. (5), for a LJ fluid having ε and σ independent of temperature, it can be shown that

$$\eta^+ = \eta_c^+ \frac{\eta}{\eta_c} \tag{19}$$

where η_c is the viscosity at the critical point, and the ratio η/η_c is the practical reduced viscosity. η_c^+ is the critical value of η^+, calculated from Eqs. (9), (11), and (15) with the parameters in Table II. The result is

$$\eta_c^+ = 0.269409 \tag{20}$$

It should be mentioned that viscosity models which, as the present one, do not account for any critical enhancement effect give a finite value for the critical viscosity. Actually, the viscosity diverges at the critical point (see,

e.g., Table C2 in Ref. 7), and the incorporation of such an effect requires a special modeling treatment [7]. Watson et al. [7] distinguished between normal viscosity and actual viscosity. The normal viscosity is equal to the actual viscosity under any condition except within a small region around the critical point. Reported "experimental" finite values for the critical viscosity should be regarded as values defined empirically by extrapolating the behavior of the normal viscosity outside the critical region smoothly into the critical region [7].

Figure 4 shows the reduced viscosity η/η_c as a function of the reduced temperature T_r at a number of values for the reduced pressure P_r. This figure is in good agreement with Fig. 1.3.1 of Bird et al. [13]. Figure 4 was generated as Fig. 3 but using Eqs. (19) and (20) instead of Eq. (16). The density values corresponding to Figs. 3 and 4 never exceeded the limits of applicability of Eq. (15).

Figures 1.3.1 and 1.3.2 of Bird et al. [13] represent two independent analyses of a large number of experimental data. On the other hand, no

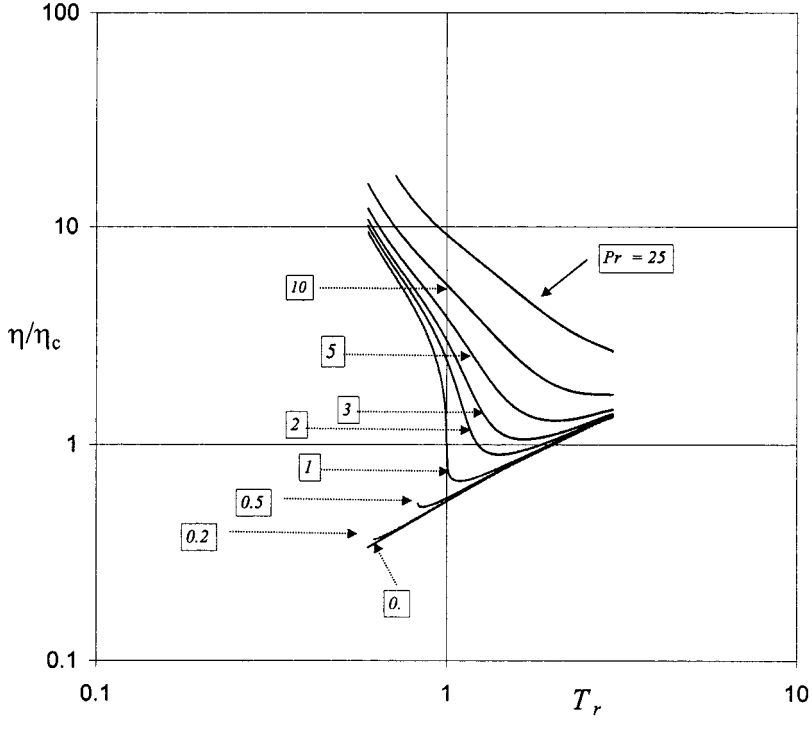

Fig. 4. Practical reduced viscosity as a function of the reduced temperature T_r for the Lennard–Jones fluid.

single real-fluid viscosity data point was used to generate the wide-ranging Figs. 3 and 4. The remarkable agreement between these figures and the figures in Ref. 13 is proof of the realism of the LJ fluid.

5. RESULTS: QUANTITATIVE ASSESSMENT

To assess more completely the potential of using the LJ analytical representation studied here as a basis for describing the viscosities of real fluids, we now concentrate on the quantitative performance of the model, by comparing model predictions against viscosity data for simple real fluids. To that end, we first need to set a criterion to assign numerical values to ε and σ for a given real fluid. The choice we made in this work is as follows. We write Eqs. (2) and (3) at the critical point. For that, we have to introduce the critical values of the dimensionless LJ variables given by Eqs. (9) and (10). Hence,

$$T_c^+ = 1.3396 = \frac{\kappa T_c}{\varepsilon} \tag{21}$$

$$P_c^+ = 0.1405 = \frac{P_c \sigma^3}{\varepsilon} \tag{22}$$

We compute the values of ε and σ from the values of the experimental critical temperature T_c and of the experimental critical pressure P_c, by solving the system of Eqs. (21) and (22). In this way, the experimental critical temperature and pressure will be exactly reproduced by the LJ PVE/hBH model [8], Eq. (8).

The advantage of this choice is that the unique behavior that takes place at the critical point, i.e., a high density-sensitivity with small changes in pressure, will be recovered by the model at a temperature equal to the experimental critical temperature.

Since even for simple fluids the true intermolecular potential can be much more complicated than the LJ function, the computed values of ε and σ have the meaning of effective LJ parameters compatible with the experimental values of the critical temperature and pressure.

We compared predicted viscosities of simple pure fluids against the data available in the compilation by Stephan and Lucas [14]. The only input experimental information used was the critical temperature, critical pressure, and molecular weight, which were also taken from Ref. 14. The parameters used in Eq. (15) were those in Table II. Table III provides a numerical calculation example.

Table III. Sample Viscosity Prediction for Oxygen at 100 K and 10 bar

Input data					
Compound	MW ($g \cdot mol^{-1}$) [14]	T_c (K) [14]	P_c (bar) [14]	T (K)	P (bar)
Oxygen	31.999	155	50.4	100	10
Calculated variables					
ε/κ (K) [Eq. (21)]	σ (Å) [Eq. (22)]	T^+ [Eq. (2)]	$\rho^+_{\text{fluid, SFE}}$ at T^+ [Eqs. (13) and (8)]	η_0^+ [Eq. (7)]	P^+ [Eq. (3)]
115.71	3.54	0.8642581	0.8966233	0.0970133	0.027877
Phase A					
Type	ρ_A^+ [Eq. (8)]	η_A^+ [Eq. (15)[a]]	η_0 (μPa · s) [Eq. (5)]	η_A (μPa · s) [Eq. (5)]	Experimental η_A (μPa · s) [14]
LIQ	0.7727073	1.9083063	7.1141776	139.9 (Prediction error: −7.2%)	150.7
Phase B					
Type	ρ_B^+ [Eq. (8)]	η_B^+ [Eq. (15)][a]	η_0 (μPa · s) [Eq. (5)]	η_B (μPa · s) [Eq. (5)]	
VAP	0.0480563	0.0999625	7.1141776	7.33	

[a] Used with the parameters in Table II.

Table IV shows the viscosity prediction results arranged according to compound and phase type (liquid, vapor, or supercritical fluid). In the calculations, the range of applicability of Eq. (15) was never exceeded for either density or temperature. Therefore, for about 2000 points available in Ref. 14, for some of the compounds in Table IV, it was not possible to compute viscosities. This issue will be the matter of future work. Results are shown for a total of 12,182 points, within the range of Eq. (15).

The results in Table IV are true predictions; i.e., the model does not use as input any single experimental real-fluid viscosity point or any

adjustable parameter obtained from experimental viscosities. The only input experimental information was the critical temperature and the critical pressure. An average error of the order of 10% should be considered low for a true prediction of viscosities over a wide range of conditions. According to this criterion, it can be seen that for simple fluids such as N_2, O_2, F_2, Ar, Kr, and Xe, the average errors are low. Average errors are also low for more complex fluids such as ethylene, propylene, carbon monoxide, carbon dioxide, methane, and ethane. For even more complex compounds, errors are often low for vapors and supercritical fluids. For instance, for supercritical bromotrifluoromethane, the average error is only 6% for 380 points, and for supercritical *n*-octane, the error is 10% for 134 points. For complex molecules, such as *n*-octane, *n*-octene, and *i*-butane, in the liquid state, the average error is large, often of the order of 30%. Despite the latter figure, we conclude, from Table IV, that it is promising to use the present approach as a basis for the viscosity modeling of real fluids, due to the low average errors obtained for simple fluids and for relatively complex fluids in supercritical and vapor states, in a purely predictive way. We stress that, at the stage of development here reported, the model is not intended to be used for the quantitative modeling of viscosities of complex real fluids.

The differentiation between components with regard to model performance is more evident for the liquid state. From Table IV, the average error for liquid viscosity is minimum for methane, oxygen, nitrogen, ethane, and fluorine, in that order. These are the types of molecules for which good results are expected by an LJ representation. Liquid propylene, *n*-heptene, and argon come next, with practically the same average error but with a smaller maximum error for argon. Argon is normally regarded as an LJ-like fluid. The higher error for liquid argon viscosity with respect to, e.g., liquid methane, may be due to several reasons. Some of them may be the effect of high-density many-body forces, which are not accounted for by the LJ intermolecular potential, accuracy differences between both viscosity databases or between the critical coordinates used to set the values of ε and σ, and fortuitous cancellations of errors. Table IV shows higher errors for the liquid viscosity of H_2 and neon. This is not surprising, since H_2 and neon are quantum fluids for which the classical mechanics approach of molecular dynamics breaks down at high enough densities and low enough temperatures [15]. Table IV also shows that the liquid viscosity error increases roughly with molecular complexity for the aliphatic hydrocarbons.

For comparison purposes, we repeated the calculations corresponding to Table IV using Eq. (6) with the original RP set of parameters b_{ji} and ω_i. The results were very similar to those in Table IV. This is not surprising

Table IV. Comparison Between Predicted Lennard–Jones Viscosities and Experimental Viscosities for Pure Compounds[a]

Name	Phase type[b]	AAD%[c]	No. of data points	Max AD%[d]	Min T_r	Max T_r	Min P_r	Max P_r
Ethylene	SCF	9	420	19	1.06	2.47	0.02	15.81
Propylene	LIQ	18	147	39	0.79	0.99	0.43	19.57
Propylene	SCF	11	420	43	1.04	1.78	0.02	19.57
Propylene	VAP	3	8	4	0.79	0.99	0.02	0.02
n-Hexene	LIQ	22	105	35	0.62	0.74	0.03	14.66
n-Heptene	LIQ	19	141	39	0.61	0.91	0.04	17.61
n-Octene	LIQ	28	123	47	0.60	0.86	0.04	19.08
Chlorodifluoromethane	LIQ	25	200	58	0.68	0.99	0.20	12.05
Dichlorodifluoromethane	VAP	16	15	83	0.65	0.99	0.02	0.49
Dichlorodifluoromethane	SCF	11	140	72	1.01	1.49	0.02	14.56
Dichlorodifluoromethane	LIQ	25	151	46	0.65	0.99	0.49	14.56
Bromotrifluoromethane	LIQ	23	172	183	0.85	0.99	0.50	15.11
Bromotrifluoromethane	VAP	3	28	8	0.85	0.99	0.03	0.76
Bromotrifluoromethane	SCF	6	380	25	1.01	1.28	0.03	15.11
Trichlorotrifluoroethane	LIQ	47	182	63	0.62	0.99	0.03	17.60
Hydrogen	VAP	19	6	20	0.64	0.91	0.08	0.08
Hydrogen	LIQ	38	43	68	0.61	0.91	0.08	23.08
Hydrogen	SCF	13	66	28	1.00	2.42	0.08	76.92
Neon	VAP	5	4	6	0.68	0.91	0.04	0.36
Neon	LIQ	26	74	31	0.68	0.91	0.36	7.27
Neon	SCF	12	390	50	1.02	2.95	0.04	7.27
Nitrogen	LIQ	14	182	29	0.63	0.99	0.29	14.71
Nitrogen	VAP	9	18	15	0.63	0.99	0.03	0.88
Nitrogen	SCF	7	574	27	1.03	2.78	0.03	29.41
Oxygen	SCF	9	612	19	1.00	2.90	0.02	19.84
Oxygen	LIQ	7	226	21	0.61	0.97	0.20	9.92
Oxygen	VAP	11	26	17	0.61	0.97	0.02	0.79
Fluorine	SCF	7	294	14	1.08	2.08	0.02	3.83
Fluorine	LIQ	15	72	27	0.63	0.97	0.38	3.83
Fluorine	VAP	4	6	4	0.63	0.97	0.02	0.02
Argon	LIQ	19	101	26	0.73	0.93	0.41	6.16
Argon	VAP	4	7	4	0.73	0.93	0.02	0.02
Argon	SCF	11	342	17	1.13	2.98	0.02	10.27
Krypton	SCF	12	284	19	1.20	2.87	0.02	9.09
Krypton	VAP	2	2	3	0.72	0.96	0.02	0.02
Xenon	SCF	13	460	22	1.03	1.48	0.02	8.56
Carbon monoxide	SCF	8	124	18	1.64	2.99	0.03	22.86
Carbon dioxide	SCF	5	495	20	1.02	2.96	0.01	13.53

i-Butane	SCF	7	544	27	1.03	2.08	0.03	13.70
i-Butane	LIQ	31	105	39	0.76	0.98	0.55	13.70
i-Butane	VAP	4	9	10	0.76	0.98	0.03	0.82
i-Pentane	LIQ	26	199	40	0.61	0.99	0.03	17.80
i-Pentane	SCF	16	264	32	1.00	1.63	0.03	17.80
i-Pentane	VAP	5	9	6	0.70	0.99	0.03	0.03
Methane	SCF	10	416	16	1.05	2.74	0.02	15.18
Methane	LIQ	5	117	23	0.61	0.95	0.43	6.51
Methane	VAP	12	11	18	0.61	0.95	0.02	0.65
Ethane	SCF	8	650	16	1.05	2.46	0.02	14.34
Ethane	LIQ	14	15	31	0.98	0.98	1.00	14.34
Propane	SCF	6	326	13	1.08	2.03	0.02	8.24
Propane	LIQ	24	185	34	0.62	0.98	0.02	8.24
Propane	VAP	4	13	9	0.65	0.98	0.02	0.71
n-Butane	SCF	6	440	21	1.06	2.00	0.03	18.42
n-Butane	LIQ	23	128	34	0.66	0.94	0.53	18.42
n-Butane	VAP	6	8	8	0.66	0.94	0.03	0.53
n-Pentane	LIQ	25	118	35	0.68	0.94	0.59	14.79
n-Pentane	VAP	4	8	12	0.68	0.94	0.03	0.59
n-Pentane	SCF	10	312	22	1.04	1.91	0.03	14.79
n-Hexane	SCF	13	280	26	1.02	1.97	0.03	16.61
n-Hexane	LIQ	28	104	44	0.75	0.98	0.66	16.61
n-Hexane	VAP	9	9	24	0.75	0.98	0.03	0.83
n-Heptane	SCF	11	170	31	1.02	1.15	0.04	18.25
n-Heptane	VAP	7	18	22	0.70	0.99	0.04	0.73
n-Heptane	LIQ	28	184	46	0.63	0.99	0.04	18.25
n-Octane	LIQ	32	160	52	0.60	0.99	0.04	20.08
n-Octane	SCF	10	134	24	1.01	1.18	0.04	20.08
n-Octane	VAP	5	16	21	0.70	0.99	0.04	0.80
i-Octane	LIQ	33	190	56	0.61	0.96	0.04	20.16

[a] LJ calculations performed using Eq. (15)/Table II. The parameters ε and σ were computed from the experimental critical temperature and pressure, this being the only experimental input information used.

[b] LIQ, liquid; VAP, vapor; SCF, supercritical fluid.

[c] Average absolute-value percentage relative deviation = $\mathrm{AAD}\% = (100/NP)\sum_{i=1}^{NP} |\eta_{\mathrm{pred}} - \eta_{\mathrm{exp}}|/\eta_{\mathrm{exp}}$.

[d] Maximum absolute-value percentage relative deviation = $\mathrm{Max\ AD}\% = \max_{i=1}^{NP}\{100\ |\eta_{\mathrm{pred}} - \eta_{\mathrm{exp}}|/\eta_{\mathrm{exp}}\}$. *NP*, number of data points; η_{pred}, predicted viscosity; η_{exp}, experimental viscosity.

since, as reported in Appendix B, the error with respect to MD LJ viscosities is similar for both models, (Eq. (15)/Table II and Eq. (6), coupled with the original RP set of parameters b_{ji}); their main difference is the way in which the Eq. (7) zero-density viscosity limit is approached (mainly at low temperatures). For the reasons we stated in the first paragraph in Section 3 and because of the tight control on the viscous qualitative behavior associated with Eq. (15)/Table II, we will use the model Eq. (15)/Table II for future development of the present modeling approach.

Figure 5 illustrates the model performance for methane, showing predicted and experimental viscosities as a function of pressure, at different temperatures. It can be seen that the predictions of the model match the experimental data very well. The intersection pressure between the 200 K isotherm and the 520 K isotherm is also properly described. Figure 6 shows viscosities as a function of pressure for *n*-octane. The model predictions here give relatively high errors for the liquid viscosity. Despite this fact, the model properly follows the experimentally observed qualitative trends reproducing the order-of-magnitude changes in viscosity. Note that the pressure and temperature ranges in Figs. 5 and 6 are wide. Despite the fact that neither methane nor *n*-octane is an LJ fluid, Figs. 5 and 6 suggest that it would be reasonable to base the modeling of the viscosities of these fluids

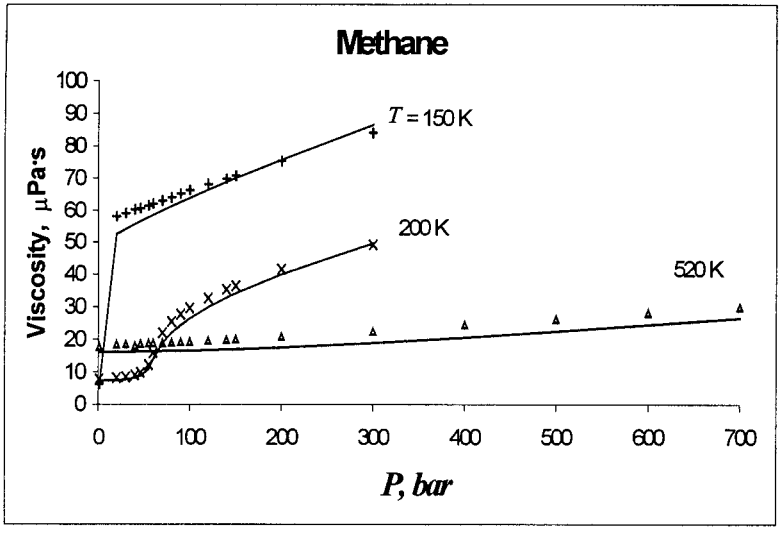

Fig. 5. Viscosity vs pressure for methane for different isotherms. Solid lines: Lennard–Jones model predictions using Eq. (15)/Table II. △, ×, and +: experimental data [14].

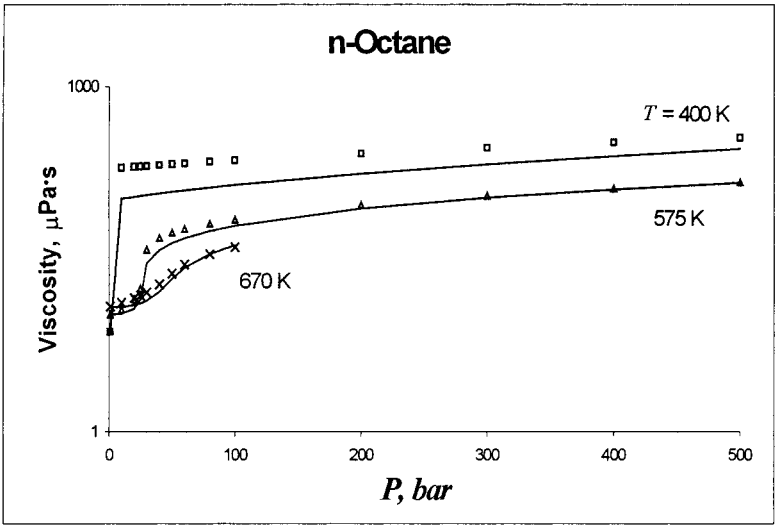

Fig. 6. Viscosity vs pressure for *n*-octane for different isotherms. Solid lines: Lennard–Jones model predictions using Eq. (15)/Table II. □, △, and ×: experimental data [14].

on the viscosities of the LJ fluid, with LJ parameters consistent with the experimental pure-compound critical temperature and critical pressure.

As is clear from Eqs. (15), (7), and (8), and as illustrated by Figs. 3 and 4, an LJ fluid is itself a corresponding-states fluid. This means, for instance, that two LJ fluids differing in their values of ε and σ will behave according to the curves in Figs. 3 and 4. On the other hand, the calculations leading to Table IV assumed that real fluids behave as LJ fluids. Therefore, the values of viscosity calculated to generate Table IV match the curves in Figs. 3 and 4. Hence, Table IV should be seen as the result of the application of a corresponding-states model where the reference fluid is an LJ fluid. The definition of the model is completed with a specific recipe to compute the values of ε and σ. According to that recipe, the only pieces of input information required to calculate viscosities are the critical temperature, critical pressure, and molecular weight. From Table IV, the present LJ-based corresponding-states model has obvious limitations. The future development of the present work will concentrate on removing those limitations.

6. CONCLUSIONS

In the present work, we studied an analytical representation of the relation among pressure, temperature, density, and viscosity for the LJ

fluid. We clearly identified its range of applicability and set convenient equations and restrictions for its parameterization. The resulting qualitative trends, over a wide range of conditions, agreed well with those of real fluids. Predictions for pure compounds were performed. Considering that they used only the experimental critical temperature and pressure as input information, error values that should be regarded as low were obtained for compounds such as N_2, O_2, F_2, Ar, Kr, Xe, ethylene, propylene, carbon monoxide, carbon dioxide, methane, and ethane, in the gaseous and dense states. For more complex compounds, errors were often low for vapors and supercritical fluids. For complex liquids, errors were relatively high, but the qualitative trends were properly described. The model was used in a truly predictive way, i.e., no adjustable parameters coming from experimental viscosities were used, and not a single viscosity data point was used as model input. Hence, we conclude that using the viscosity of LJ fluids, over wide ranges of pressure and temperature, as a basis for the viscosity modeling of real fluids is promising. In the future, suitable modifications will be introduced to describe the viscous behavior of complex fluids better.

APPENDIX A: THE KOLAFA–NEZBEDA LJ EOS

The PVE/hBH LJ EOS of Kolafa and Nezbeda (KN) [8] is the following:

$$z = \frac{P^+}{\rho^+ T^+} = f_{\mathrm{KN}}(\rho^+, T^+) \tag{8}$$

where

$$f_{\mathrm{KN}}(\rho^+, T^+) = z_{\mathrm{HS}} + z_{\mathrm{VIR}} + z_{\mathrm{RES}} \tag{A1}$$

with

$$z_{\mathrm{HS}} = \frac{1 + \tau + \tau^2 - 2/3\tau^3(1+\tau)}{(1-\tau)^3} \tag{A2}$$

$$\tau = \frac{\pi \rho^+ d_{\mathrm{hBH}}^3}{6} \tag{A3}$$

$$d_{\mathrm{hBH}} = \sum_i C_{d,i}(T^+)^{i/2} + C_{d,\ln}\ln(T^+) \tag{A4}$$

$$z_{\mathrm{VIR}} = \Delta B_{2,\mathrm{hBH}} \rho^+ \lfloor 1 - 2\gamma(\rho^+)^2 \rfloor \exp\lfloor -\gamma(\rho^+)^2 \rfloor \tag{A5}$$

$$\Delta B_{2,\mathrm{hBH}} = \sum_i C_{\mathrm{VIR},i}(T^+)^{i/2} \tag{A6}$$

$$z_{\mathrm{RES}} = \sum_i \sum_j j C_{ij} (T^+)^{(i/2-1)} (\rho^+)^j \tag{A7}$$

Table AI. Coefficients for Eqs. (A4) to (A6)

Equation (A4)	
i	$C_{d,i}$
−2	0.011117524
−1	−0.076383859
0	1.080142248
1	0.000693129
ln	−0.063920968
Equation (A5)	
γ	1.92907278
Equation (A6)	
i	$C_{\mathrm{VIR},i}$
−7	−0.58544978
−6	0.43102052
−5	0.87361369
−4	−4.13749995
−3	2.90616279
−2	−7.02181962
0	0.02459877

The values of the constants for Eqs. (A4) to (A7) are given in Tables AI and AII.

APPENDIX B: MODIFICATION OF THE LENNARD–JONES VISCOSITY ANALYTICAL REPRESENTATION

Figure B1 shows two LJ supercritical isotherms computed using Eq. (6) coupled with the original RP set of parameters b_{ji} and ω_i. It depicts the following viscous behavior.

(a) At a constant temperature, viscosity increases with density;

(b) At zero density, viscosity increases with temperature. In contrast, at high densities, viscosity decreases with temperature;

(c) At zero density, the viscosity is less at $T^+ = 1.8$ than at $T^+ = 4$. At $T^+ = 1.8$, the viscosity increases with density more rapidly than the viscosity at $T^+ = 4$. Hence, the isotherms intersect each other at a high enough density;

Table AII. Coefficients for Eq. (A7)

i	j	C_{ij}
0	2	2.01546797
0	3	−28.17881636
0	4	28.28313847
0	5	−10.42402873
−1	2	−19.58371655
−1	3	75.62340289
−1	4	−120.70586598
−1	5	93.92740328
−1	6	−27.37737354
−2	2	29.34470520
−2	3	−112.35356937
−2	4	170.64908980
−2	5	−123.06669187
−2	6	34.42288969
−4	2	−13.37031968
−4	3	65.38059570
−4	4	−115.09233113
−4	5	88.91973082
−4	6	−25.62099890

(d) At a constant temperature, the viscosity curves are flat at low densities and steeper at high densities, i.e., the slope of η^+ vs ρ^+ at a constant temperature increases with density.

The viscous behavior in Fig. B1 is in essential agreement with that of real fluids. However, the previous list of statements is biased to some extent by the scale of Fig. B1 and by the temperature values chosen.

Let us look at a lower-temperature isotherm. Figure B2 shows the original MD RP LJ viscosity data for $T^+ = 0.8$, together with the corresponding η^+-vs-ρ^+ curve computed at $T^+ = 0.8$ using Eq. (6) with the original RP set of parameters b_{ji} and ω_i. It can be seen, for both the data and the curve, that there is a minimum in viscosity in the low-density region. It can also be seen that the zero-density limit is approached with a notably negative η^+-vs-ρ^+ slope. Most of the MD data shown in Fig. B2 actually fall within the two-phase region, and hence they correspond to a metastable LJ fluid. According to Rowley and Painter [5], "Simulations were performed in the two-phase region only to provide continuity of states between vapor and liquid densities in anticipation of correlating the data

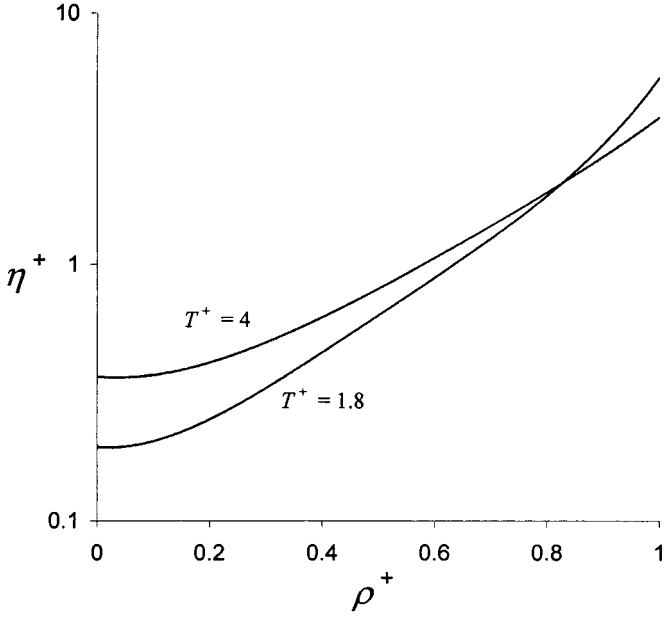

Fig. B1. Lennard–Jones viscosity η^+ as a function of density ρ^+ for two supercritical isotherms. The isotherms were computed using Eq. (6) coupled with the original RP set of parameters b_{ji} and ω_i.

into polynomial equations. Values in the two-phase region have no other significance." Hence, the justification for the minimum in Fig. B2 is weak. By producing viscosity values in the metastable region, the authors probably intended to avoid unphysical oscillations in the polynomial fitting function [Eq. (6)]. It should be noted that Eq. (6) represents the LJ viscosity as a continuous function of density, at any given temperature. This means that within the (subcritical) two-phase region, Eq. (6) provides viscosity values of a hypothetically homogeneous equilibrium LJ fluid or of a metastable homogeneous LJ fluid. This has clear advantages as discussed by Vesovic et al. [17]. Despite the weak justification for the minimum in Fig. B2, homogeneous real fluids can have a viscous behavior qualitatively similar to that in Fig. B2. For real fluids, the viscosity-vs-density slope at zero density is in general different from zero. It can change sign from positive to negative as the temperature is reduced [18]. At subcritical temperatures, the sign is normally negative. In such a case "the viscosity along an isotherm should first decrease in the vapor phase and subsequently increase with increasing density" [6]. A minimum may or may not occur, depending on the location of the two-phase boundary [6].

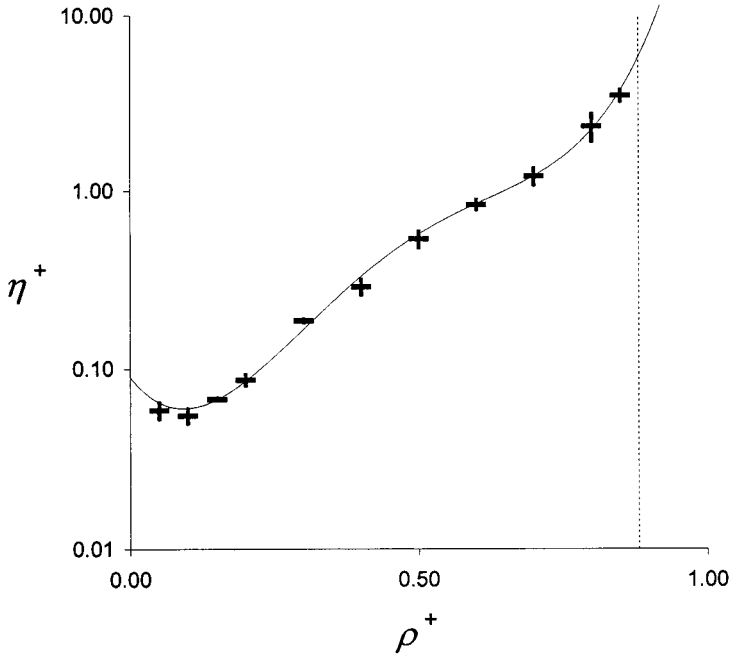

Fig. B2. Lennard–Jones viscosity η^+ as a function of density ρ^+ at $T^+ = 0.8$. Solid line: computed using Eq. (6) coupled with the original RP set of parameters b_{ji} and ω_i. Vertical dashed line: fluid density at solid–fluid equilibrium. (+) MD RP LJ data [5]. The height of the plus symbols corresponds to the uncertainties reported by Rowley and Painter [5].

For an LJ fluid having ε and σ independent of temperature, it can be shown, from Eq. (2), that

$$T^+ = T_r T_c^+ \tag{B1}$$

where T_c^+ is a constant [Eq. (9)] and T_r is the practical reduced temperature, defined as

$$T_r = \frac{T}{T_c} \tag{B2}$$

where T_c is the critical temperature. A chosen value of T_r automatically sets a value for T^+ through Eq. (B1).

Consider the product $(\rho_c/\eta_0)(\partial\eta/\partial\rho)_0$, where ρ_c is the critical density and subscript 0 stands for the zero-density limit. $(\partial\eta/\partial\rho)_0$ is the derivative of viscosity with respect to density at zero density, i.e., the initial slope for

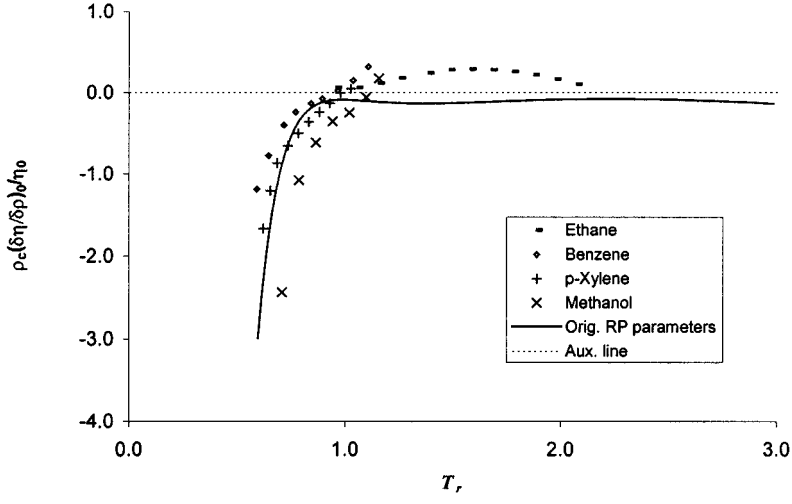

Fig. B3. Dimensionless zero-density viscosity-vs-density slope as a function of practical reduced temperature. Solid line: Eq. (6), with the original RP set of parameters b_{ji} and ω_i, at zero density, coupled with Eqs. (7) and (11). Experimental data: ethane [23]; benzene and methanol [21]; *p*-xylene [24]. Experimental critical densities were obtained from Ref. 25.

the viscosity dependence with respect to density. For a chosen value of T_r, the product $(\rho_c/\eta_0)(\partial\eta/\partial\rho)_0$ can be computed using Eqs. (B1), (6), (7), and (11). The dimensionless product $(\rho_c/\eta_0)(\partial\eta/\partial\rho)_0$ can be calculated with the model without having to specify values for ε and σ.

Figure B3 shows the product $(\rho_c/\eta_0)(\partial\eta/\partial\rho)_0$ as a function of reduced temperature both for the LJ model corresponding to Eq. (6) with the original RP set of parameters b_{ji} and ω_i and for real fluids (experimental values). Figure B3 shows that the model gives always a negative zero-density viscosity-vs-density slope throughout the temperature range of Eq. (6). For reduced temperatures higher than unity, the model slope value is very close to zero. For real fluids, it is shown in Fig. B3 that the initial slope can be negative or positive, depending on the temperature range.

The nonzero viscosity-vs-density slope observed at zero density for real fluids is a minor effect. For instance, for propane [6] the appearance of low-density minima at subcritical temperatures is at most a 1% effect. This number is 1.8% for some refrigerants [19, 20], 3% for ammonia [18], and 3% for water [7]. On the other hand, the minimum in Fig. B2 corresponds roughly to a 30% decrease in viscosity with respect to the zero-density value. Such an overestimation of the minimum probably comes from having used MD simulation data corresponding to a

metastable LJ fluid. Additionally, for real fluids, the magnitude of the viscosity-vs-density slope at low densities is in most cases much smaller than the slope at high density.

As stated in the text, we foresee the need to set proper extrapolation schemes for computing reference LJ viscosities under conditions falling outside the range of applicability of Eqs. (6) and (8), during the future development of the present model. The relatively involved behavior shown in Fig. B2 complicates the setting of robust extrapolation schemes. On the other hand, the minimum-viscosity effect is small for real fluids. Hence, we decided to replace Eq. (6) by Eq. (15), which forces the viscosity-vs-density slope to be zero at zero density, and to impose on the general LJ adjustable parameters of Eq. (15) other restrictions consistent with statements (a) to (d) above.

We screened out, from the MD LJ data set used as input for the refitting process, the three RP MD LJ viscosity data clearly responsible for the minimum shown in Fig. B2. The three removed data correspond to $T^+ = 0.8$ and to the following values of ρ^+: 0.05, 0.1, and 0.15. Note that for the refitting process, we considered as valid the η_0^+ values calculated with Eq. (7).

In the following we present in detail the simplifying restrictions imposed on the fitted parameters of Eq. (15). The restrictions stem from statements (a) to (d) above, which arose from Fig. B1.

The flatness of the η^+-vs-ρ^+ curve at $\rho^+ = 0$ corresponds to

$$\left(\frac{\partial \eta^+}{\partial \rho^+}\right)_0 = 0 \tag{B3}$$

where the subscript 0 implies that the partial derivative of Eq. (B3) is evaluated at zero density. It can be shown that Eq. (15) of the text satisfies Eq. (B3) at any temperature T^+. The reason is that the argument of the exponential function in Eq. (15) has no constant or linear terms with respect to the density ρ^+. We used Eq. (15) to fit the parameters reported in Table II and in all further calculations. Due to Eq. (15), the number of adjustable parameters is now less than the number of parameters of the original Rowley and Painter [5] fit of Eq. (6).

The monotonic increase in viscosity with density at a constant temperature, adopted as the basic reference behavior, is expressed by

$$\frac{\partial \eta^+}{\partial \rho^+} > 0 \qquad \text{for} \quad \rho^+ > 0 \tag{B4}$$

The increase in the η^+-vs-ρ^+ slope with density is set by

$$\frac{\partial(\partial\eta^+/\partial\rho^+)}{\partial\rho^+} > 0 \qquad \text{for} \quad \rho^+ \geqslant 0 \tag{B5}$$

The faster increase in viscosity with density that takes place at lower temperatures implies that, at a given density (different from zero), the slope $\partial\eta^+/\partial\rho^+$ has to decrease with temperature, i.e.,

$$\frac{\partial(\partial\eta^+/\partial\rho^+)}{\partial T^+} < 0 \qquad \text{for} \quad \rho^+ > 0 \tag{B6}$$

We used inequalities (B4) to (B6) for fitting the parameters of Eq. (15). The objective function was based on the relative errors with respect to the RP MD LJ viscosity data. Rowley and Painter [5] have not reported any use of restrictions such as Eqs. (B4) to (B6) for their original fitting of the coefficients of Eq. (6) of the text.

Note that the restriction (B4) is not set at zero density because Eq. (15) implies a zero slope at zero density. The inequality (B5) has to be met even at zero density. At zero density, the inequality (B6) does not apply: since Eq. (15) implies a zero slope at zero density, and at any temperature, the derivative $\partial(\partial\eta^+/\partial\rho^+)/\partial T^+$ equals zero at zero density.

Compliance with the previous restrictions ensures the absence of problematic loops in the two-phase region, thus securing a smooth path from the slowly varying low-density viscosity values to the dramatic viscosity rise in the dense region. This issue has been discussed by Vogel et al. [6]. The previous restrictions imply that $(\eta^+ - \eta_0^+)$-vs-ρ^+ isotherms will all merge as the density tends to zero, while at high densities, they will be fully stratified.

Table II presents the set of parameters for Eq. (15). They produce an average absolute relative deviation of 6.1% with respect to the RP MD LJ viscosity data (168 accepted points). The bias is -0.77%. These values are similar to those reported for the original RP parameters (171 points) [5].

The parameters in Table II are such that the inequalities (B4) to (B6) are satisfied under all temperature–density conditions of the MD RP LJ viscosity data. We also tested the absence of violations to the restrictions in Eqs. (B4) to (B6) for more than 12,000 regularly spaced points in a section of the temperature–density plane defined by the ranges $0.8 \leqslant T^+ \leqslant 4$ and $0 \leqslant \rho^+ \leqslant 1$.

Equation (B3) sets the low-density viscosity-vs-density slope to be zero. This is acceptable for our modeling purposes. However, the reader

should bear in mind that, to get the zero-density viscosity η_0 for a real fluid from experimental information, it is of utmost importance to determine the value of the low-density viscosity-vs-density slope [21], which is normally different from zero. The real-fluid viscosity η_0 is then obtained through extrapolation to the limit of zero density; i.e., η_0 is not an "experimentally accessible quantity" [6]. Forcing the zero-density viscosity-vs-density slope to be zero, as set by Eq. (B3), implies that the model will predict a second viscosity virial coefficient, B_η [21], equal to zero. This would not be acceptable had the goal been to represent well B_η. Our goals do not include the description of B_η. A previous work where a zero value of B_η was also set is that by Younglove and Ely [22], for the case of propane [6].

Equation (15) coupled with the set of constants in Table II is consistent with the vast majority of the RP LJ viscosity data. With regard to real fluids, these constants give a qualitative behavior simpler than that observed. However, they provide a reference viscosity description with well-defined qualitative trends, grasping the essential known viscous behavior of fluids. In this way, the user can keep control on the expected model behavior. Corrections can potentially be added to this reference model to account for more complex phenomena, such as some real-fluid abnormal phenomenological behavior. For instance, the tabulated values of viscosity for dense water [7] show a minimum in viscosity as a function of density, for the metastable liquid at 0°C and at atmospheric pressure.

ACKNOWLEDGMENTS

The authors are grateful to Mr. José Joaquim Barros Machado for helping to prepare the digital version of the viscosity database used here; to Professor R. L. Rowley (Brigham Young University) for his kind e-mail collaboration; to Professor Erling H. Stenby and Mr. Claus Zéberg-Mikkelsen (Technical University of Denmark) for having provided, within the framework of the European project EVIDENT, a database used for preliminary calculations; and to Dr. V. Vesovic (Imperial College of Science, Technology and Medicine) for useful exchange of information during the 18th European Seminar on Applied Thermodynamics. The authors are also indebted to the European Commission (EVIDENT project, Contract JOF3-CT97-0034) and to Consejo Nacional de Investigaciones Científicas y Técnicas de la República Argentina.

NOMENCLATURE

AAD%	Average absolute-value percentage relative deviation
B_η	Second viscosity virial coefficient

k	Boltzmann constant
LIQ	Liquid
m	Mass of one molecule
Max AD%	Maximum absolute-value percentage relative deviation
N	Number of molecules
N_A	Avogadro's number
NP	Number of data points
P	Absolute pressure
P_c	Critical pressure
P_r	Practical reduced pressure
P^+_{SFE}	LJ melting P^+
PVT	Pressure–volume–temperature
r	Intermolecular distance
SCF	Supercritical fluid
SFE	Solid–fluid equilibrium
T	Absolute temperature
T_c	Critical temperature
T_r	Practical reduced temperature
u	Potential energy
V	System volume
VAP	Vapor
VLE	Vapor–liquid equilibrium
z	Compressibility factor

Greek Letters

ε	Depth of the LJ potential well
η	(Newtonian shear) viscosity
η_0	Viscosity at zero density
η_c	(Normal) critical viscosity
η_{exp}	Experimental viscosity
η_{pred}	Predicted viscosity
$\rho^+_{fluid,\ SFE}$	Dimensionless density of a dense LJ fluid in equilibrium with an LJ solid
ρ	Amount-of-substance density (as, e.g., $mol \cdot cm^{-3}$)
ρ_c	Critical amount-of-substance density (as, e.g., $mol \cdot cm^{-3}$)
σ	LJ separation distance at zero energy

REFERENCES

1. J. M. Haile, *Molecular Dynamics Simulation. Elementary Methods* (John Wiley, New York, 1997).
2. S. Murad, *AIChE J.* **32**:513 (1986).

3. T. Sun and A. S. Teja, *Ind. Eng. Chem. Res.* **37**:3151 (1998).
4. K. E. Gubbins, in *Models for Thermodynamic and Phase Equilibria Calculations*, S. I. Sandler, ed. (Marcel Dekker, New York, 1994).
5. R. L. Rowley and M. M. Painter, *Int. J. Thermophys.* **18**:1109 (1997). [Note: See information on errors following Eq. (7) in the present article.]
6. E. Vogel, C. Kuchenmeister, E. Bich, and A. Laesecke, *J. Phys. Chem. Ref. Data* **27**:947 (1998).
7. J. T. R. Watson, R. S. Basu, and J. V. Sengers, *J. Phys. Chem. Ref. Data* **9**:1255 (1980).
8. J. Kolafa and I. Nezbeda, *Fluid Phase Equil.* **100**:1 (1994).
9. M. Mecke, A. Müller, J. Winkelmann, J. Vrabec, J. Fischer, R. Span, and W. Wagner, *Int. J. Thermophys.* **17**:391 (1996). Also, *Int. J. Thermophys.* **19**:1493 (1998), Erratum 1.
10. M. S. Zabaloy and J. H. Vera, *Ind. Eng. Chem. Res.* **35**:829 (1996).
11. R. J. Topliss, D. Dimitrelis, and J. M. Prausnitz, *Computers Chem. Eng.* **12**:483 (1988).
12. R. Agrawal and D. A. Kofke, *Mol. Phys.* **85**:43 (1995).
13. R. B. Bird, W. E. Stewart, and E. N. Lightfoot, *Transport Phenomena* (John Wiley, New York, 1960), pp. 16–17.
14. K. Stephan and K. Lucas, *Viscosity of Dense Fluids* (Plenum Press, New York and London, 1979).
15. J. P. Hansen and I. R. McDonald, *Theory of Simple Liquids* (Academic Press, London, 1976), p. 1.
16. R. L. Rowley, *Personal communication* (May 19, 1999).
17. V. Vesovic, M. J. Assael, and Z. A. Gallis, *Int. J. Thermophys.* **19**:1297 (1998).
18. A. Fenghour, W. A. Wakeham, V. Vesovic, J. T. R. Watson, J. Millat, and E. Vogel, *J. Phys. Chem. Ref. Data* **24**:1649 (1995).
19. M. Takahashi, C. Yokoyama, and S. Takahashi, *J. Chem. Eng. Data* **32**:98 (1987).
20. M. Takahashi, N. Shibasaki-Kitakawa, C. Yokoyama, and S. Takahashi, *J. Chem. Eng. Data* **40**:900 (1995).
21. E. Vogel, E. Bich, and R. Nimz, *Physica* **139A**:188 (1986).
22. B. A. Younglove and J. F. Ely, *J. Phys. Chem. Ref. Data* **16**:577 (1987).
23. S. Hendl and E. Vogel, *Fluid Phase Equil.* **76**:259 (1992).
24. E. Vogel and S. Hendl, *Fluid Phase Equil.* **79**:313 (1992).
25. *DIPPR 801*, *Evaluated Process Design Data*, *Public Release* (American Institute of Chemical Engineers, Design Institute for Physical Property Data, BYU-DIPPR, Thermophysical Properties Laboratory, Provo, UT, 1998).